This is the submitted version of the article:

Morresi T., Binosi D., Simonucci S., Piergallini R., Roche S., Pugno N.M., Simone T.. Exploring event horizons and Hawking radiation through deformed graphene membranes. 2D Materials, (2020). 7. 041006: - . 10.1088/2053-1583/aba448.

Available at: https://dx.doi.org/10.1088/2053-1583/aba448

Forging graphene pseudospheres to mimic curved spacetimes

Tommaso Morresi,[1,2] Daniele Binosi,[1] Stefano Simonucci,[3] Riccardo Piergallini,[3] Stephan Roche,[4*] Nicola M. Pugno,[2,5,6] Simone Taioli[1,7*]

[1]European Centre for Theoretical Studies in Nuclear Physics and Related Areas (ECT*-FBK), Trento, Italy [2]Laboratory of Bio-Inspired & Graphene Nanomechanics - Department of Civil, Environmental and Mechanical Engineering, University of Trento, Italy [3]School of Science and Technology, University of Camerino, Camerino, Italy [4]Institut Catal de Nanociència i Nanotecnologia - ICN2, Barcelona, Spain [5]Ket-Lab, Edoardo Amalfi Foundation, Rome, Italy [6]School of Engineering and Materials Science, Materials Research Institute - Queen Mary University of London, London, UK [7]Trento Institute for Fundamental Physics and Applications (TIFPA-INFN), Trento, Italy

Quantum mechanics and general relativity are among the most successful theories of modern physics. Each and every phenomena that they have predicted, from entanglement to black holes, has been experimentally tested and verified. On the other hand, some tension exists when the two theories are unified in a single framework, which, in turn, makes it extremely challenging to obtain firm theoretical predictions. Perhaps, the only exception is the discovery by Hawking that, from a quantum mechanical point of view, black holes are not completely black[1]: they emit 'Hawking radiation' consisting of photons, neutrinos and, to a lesser extent, all sorts of massive particles. However, direct detection of this radiation, which is thermal in nature, is unlikely: the latter is proportional to the inverse of the black hole mass, which, for the smallest observed black hole, implies $T = 60$ nK which is 9 orders of magnitude smaller than the current cosmic microwave background temperature. On the other hand, so-called black hole analogues, first proposed by Unruh[2], are rapidly turning from promising to consolidated avenues in the study of various thermodynamics aspects. This is particularly true for sonic analogues built from ultracold gases[3–12], for which not only spontaneous Hawking radiation has been experimentally observed[13], but also its correlation spectrum shown to be thermal and with a temperature given by the system's surface gravity[14], thus vindicating Hawking's predictions. The state-of-the-art for solid-state black hole analogues is at a less advanced state[15]: while all current experimental approaches face major challenges mainly related to material synthesis and device fabrication, in the last couple of years key conceptual advances have been achieved that show hopes for some of the fundamental questions to be addressed in these systems too, especially in conjunction to the implementation of the Sachdev-Ye-Kitaev model[16,17]. Here we construct a solid-state black-hole analogue consisting of a graphene crystal with a three-connected tessellation engineered to shape it in the form of a constant negative curvature surface, known as a Beltrami's pseudosphere[18,19]. We develop a novel computational method to build realistic negative curvature carbon structures comprising several million atoms; and devise a tight-binding (TB) approach to calculate the local density of state (LDOS) for these extended curved structures. Comparison between the numerically evaluated LDOS and the theoretically predicted one shows, within uncertainties, its thermal nature, establishing the presence of a black hole type horizon in the device.

Beltrami's pseudosphere represents the hyperbolic counterpart of the regular sphere: it is a surface of revolution characterized by a constant negative Gaussian curvature $\kappa = -1/R_{\rm p}^2$, with $R_{\rm p}$ the pseudosphere radius. Gauss Bonnet's theorem shows immediately that a carbon allotrope arranged in a pseudosphere shape requires the presence of Stone-Wales (SW) defects with heptagonal defects exceeding the pentagonal ones by exactly six units. In addition, Hilbert's theorem states that no analytic complete surfaces of constant negative Gaussian curvature can be embedded in $\mathbb{R}^3$, so that a graphene pseudosphere will be neither compact nor finite. Insights for finding a (local) minimum energy tiling of the Beltrami's pseudosphere has been offered in[20]; but this study was inconclusive in: i) delivering a general approach to the tessellation of hyperbolic surfaces; ii) scaling-up the graphene pseudosphere size; iii) measuring the surface's electronic structure. And properties ii) and iii) will be of paramount importance in ascertain the capacity of the structure to act as an analogue gravity model (see below). We start the structure generation from a planar graphene sheet, in which we force the presence of six heptagonal faces in the center (see Fig. 1a panel i). The initial configuration of the pseudosphere (Fig. 1a panel ii) is then obtained by simply projecting the graphene net on the Beltrami's surface along the z-axis (see Methods), and shows carbon-to-carbon bond lengths in the flat (curved) regions which are shorter (longer) than the typical bond distances in graphene ($a_{\rm CC} = 0.142$ nm). A sequence of bond-switching trial moves and structural optimization steps with a modified Keating potential to favour the formation of hexagonal cells, is then applied (see Methods), and accepted/rejected according to an energy-minimization criterion (Fig. 1a, panels iii through v). After $\mathcal{O}(10^4)$ moves the algorithm efficiency drastically drops, which limits the radius size of the minimized structures (panel vi) to few nm and the number of carbon atoms to $\mathcal{O}(10^3)$. Scaling up of the numbers of atoms

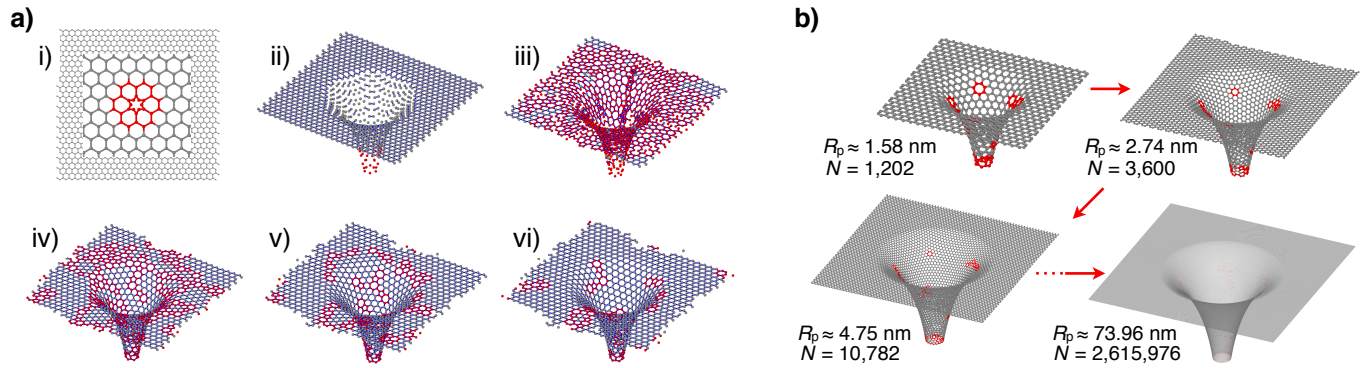

FIG. 1. a) Optimization of a carbon pseudosphere containing $N = 1626$ atoms with radius $R_p = 18.26$ Å. Panels from i) to vi) represent different optimization stages, consisting of trial bond switch–twist moves. Carbon atoms that do not belong to the hexagonal faces are marked in red color. Starting from an initial configuration (panel i) almost entirely tiled with hexagonal polygons, atoms rearrange to fill uniformly the surface reaching a local minimum after a few thousands steps (panel iv). After reaching this configuration, trial moves are rejected at an increasingly high rate and the Metropolis algorithm becomes inefficient. b) A dualization sequence (described in Methods), leading to a thousandfold increase in the number of carbon atoms and close to a hundredfold increase in the pseudosphere radius.

is next implemented through a custom dualization algorithm (Fig. 1b), by which the pseudosphere radius and number of atoms scale like $\sim \sqrt{3}$ and ~ 3 respectively, while conserving both the bond distance as well as the number of defects (see Methods). Each dualization step is next followed by a bond switching optimization run to counteract the former tendency of splitting apart the SW defects of the original structure and thus artificially increasing its total energy. Repeated application of this procedure allows to reach a thousandfold increase in the number of carbon atoms ($N = 2,615,976$) and a pseudosphere radius $R_{\rm p} = 73.96$ nm.

Next, the electronic properties of these structures can be characterized in terms of the LDOS near the Dirac points[21] where electrons behave as relativistic massless pseudo-particles. Given the $\mathcal{O}(10^6)$ carbon atoms of the structures realized, the LDOS will be evaluated through a multi-orbital Tight Binding (TB) approach implementing the Kernel Polynomial Method (KPM) to avoid the diagonalization of the Hamiltonian. Due to curvature, the p_z orbitals forming the π band are not anymore orthogonal to the in-plane direction; the same happens for the sp^2-hybridized orbitals, which do not lay in the graphene plane. Thus, a multi-orbital TB approach, in which all four valence orbitals $(2s, 2p_x, 2p_y, 2p_z)$ are included in the simulation as opposed to the p_z orbital alone, has been employed (see Methods, where details concerning the parametrization of the Hamiltonian are reported and well-established results on graphene and carbon nanotube structures reproduced). The LDOS projected onto longitudinal circles in regions located at a different z-depth along pseudospheres obtained at various stages of the dualization procedure (and thus characterized by varying number of atoms N and radius $R_{\rm p}$), is plotted in Fig. 2. In each case we evaluate the LDOS for three different structures differing by the number and location of the SW defects. In the energy range $E \in [-6, 6]$ eV, the LDOS shows a graphene-like shape for all the pseudospheres independently of the radius and defect distribution. With respect to the pristine graphene region i), region ii), shows Van-Hove singularities associated to the π band peaks which are broadened and shifted; this is due to the slightly elongated carbon bonds characterizing this region, which represents the would-be Hilbert horizon (where the pseudosphere ends as a consequence of Hilbert theorem) of the pseudosphere. After that, the LDOS stays the same at a qualitatively level independently from the depth inside the pseudosphere's 'throath' at which it is evaluated. A similar behaviour (Fig. 3 a) persists in the biggest structures studied, which also confirms that the bulge happening in the vicinity of the Fermi energy seen in the blown up region in Fig. 3 a), and which could be also already seen in the central region of Fig. 2), is a genuine curvature effect. Projecting the LDOS over single atomic sites both inside and outside the pseudosphere (sites s_{1-5} in Fig. 3 b)) and separating out the nearest neighbours contributions (that would correspond to the A and B sublattices in pristine graphene), we find that the LDOS spectrum around the Fermi energy is significantly asymmetric for the two nonequivalent sublattices while for $E \gg E_{\rm F}$ it is practically indistinguishable.

The largest simulated pseudosphere has a ratio $a_{\rm CC}/R_{\rm p} \sim 2\times10^{-3}$, which quantifies how well the Hilbert horizon and the Rindler-type event horizon emerging when treating the pseudosphere as a 2+1 dimensional space-time coincide[19] (0 representing coincidence). In the ideal case[18,19], in the vicinity of the horizon Hawking radiation takes place with the massless electron's action before (respectively after) tunnelling has taken place be-

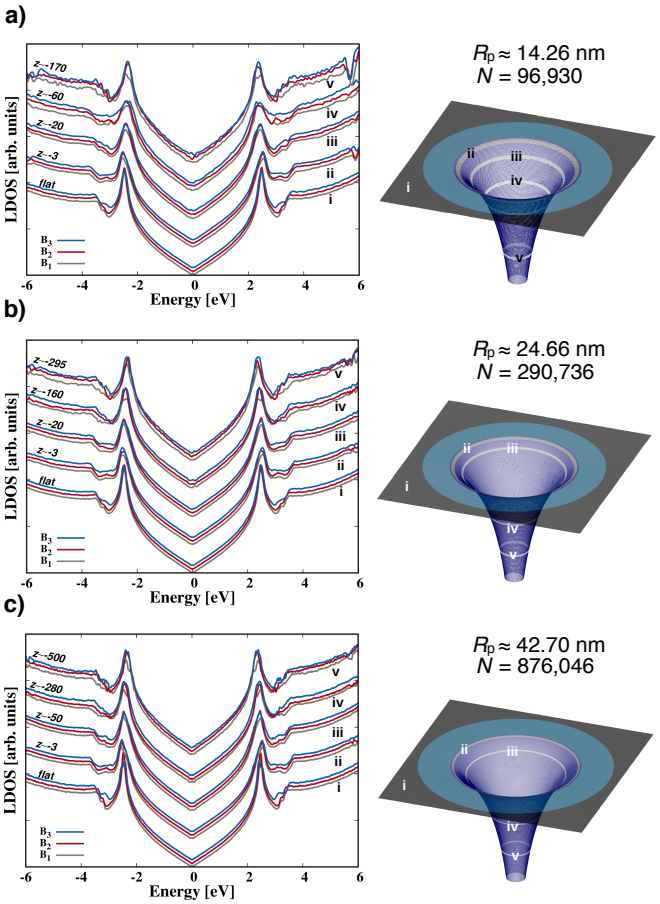

FIG. 2. Panels a) through c): LDOS projected onto five regions at different depth along the revolution axis z (i through v) for various pseudospheres characterized by three different values of the number of atoms N, radius R_p. For each case of N and R_p we report the LDOS for three pseudosphere realizations B_{1-3} differing by the configurations of SW defects, of which a representative is shown on the right of each panel. The Fermi energy is set equal to zero in all cases.

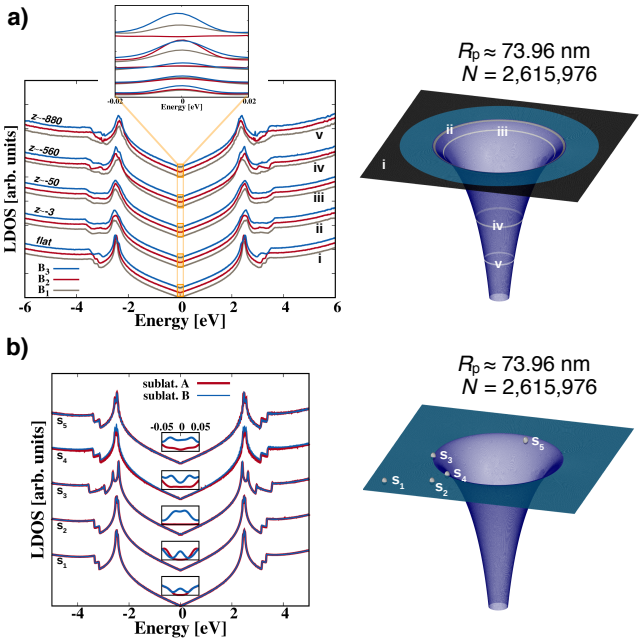

FIG. 3. a) Same as before but for the three biggest pseudospheres ($N = 2,615,976$ and $R_\mathrm{p} = 73.96$ nm, right). We also zoom on the Fermi energy to expose the LDOS bulge in this region. b) Pseudosphere's LDOS projected over the shown sites s_i. Projection over the two would-be inequivalent sublattices A and B of graphene is shown; the insets zoom near the Fermi energy to show the LDOS asymmetry.

ing

$$S = i v_\mathrm{F} \int \mathrm{d}^3x \, \sqrt{g} \bar{\psi} \gamma^\mu \mathcal{D}_\mu \psi, \tag{1}$$

with: $v_\mathrm{F} \sim c/300$ the Fermi velocity; γ the Dirac matrices; $\mathcal{D}_\mu$ the SO(2,1) (respectively, flat) covariant derivative; and, finally, g the determinant of the pseudosphere metric (respectively 1) with (conformal) metric $\mathrm{d}s^2_\mathrm{B} = \phi^2(u)\mathrm{d}s^2_\mathrm{R}$, where $\phi(u) = \ell/r \; \mathrm{e}^{u/r}$ (with ℓ a constant that in the physical case is to be indentified with a_CC) and $\mathrm{d}s^2_\mathrm{R}$ is the Rindler-type metric $\mathrm{d}s^2_\mathrm{R} = \phi^{-2}(u)(\mathrm{d}t^2 - \mathrm{d}u^2) - r^2\mathrm{d}v^2$. ($u$ and v are the curvilinear coordinates spanning the pseudosphere). Hawking radiation is then characterized by a LDOS obtained by evaluating the power spectrum ρ of the 2-point function $S_\mathrm{B} = \langle 0_\mathrm{M}|\psi_\mathrm{B}\bar{\psi}_\mathrm{B}|0_\mathrm{M}\rangle$ with $|0\rangle_\mathrm{M}$ the flat vacuum. If an event horizon is present, then it would be revealed by the the thermal nature of the power spectrum, since[18,19], neglecting boundary terms,

$$\rho = \frac{4}{\pi} \frac{1}{(\hbar v_\mathrm{F})^2} \frac{R_\mathrm{p}^2}{a_\mathrm{CC}^2} \mathrm{e}^{-2u/R_\mathrm{p}} \frac{E}{\mathrm{e}^{\frac{E}{\kappa\Theta}} - 1}; \quad \Theta = \frac{\hbar v_\mathrm{F}}{\kappa} \frac{a_\mathrm{CC}}{2\pi r^2} \mathrm{e}^{u/r}, \tag{2}$$

where κ is the Boltzman constant and Θ the temperature, which reaches its maximum at the horizon where $r = R_\mathrm{p}$, $u = R_\mathrm{p} \ln R_\mathrm{p}/a_\mathrm{CC}$, and $\Theta = \hbar v_\mathrm{F}/2\pi\kappa R_\mathrm{p} \sim 16$ K for our largest pseudosphere. Notice in addition that only electrons with an energy $E = \hbar v_\mathrm{F}/R_\mathrm{p} \sim 9$ meV have a long enough wavelength to experience the effects of the curvatures and thus 2. Given the exponential nature of the power spectrum (2), the effect of the presence of the horizon should manifest in a marked asymmetry of the LDOS around the Fermi energy, as measured by the contrast

$$\nu = \left| \frac{\mathrm{LDOS}_{E<0} - \mathrm{LDOS}_{E>0}}{\mathrm{LDOS}_{E<0} + \mathrm{LDOS}_{E>0}} \right|. \tag{3}$$

Results for the LDOS and its contrast projected on sites located near the Hilbert/Rindler horizon are shown in Fig. 4. The behavior of the curves is remarkably similar; recall, in fact, that the continuum approximation

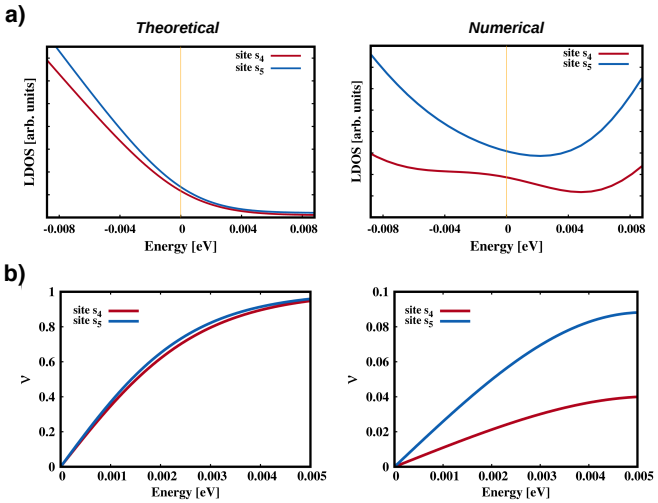

FIG. 4. a) LDOS lineshape and contrast projected over the pseudosphere sites $s_{4,5}$ shown in Fig. 3 b), according to analytical predictions[22,23] and numerical results.

formula (2) is valid when neglecting both local elastic effects induced by the curvature as well as the presence of SW defects; and that in our computational model, the interplay between curvature and defects (which the Gauss-Bonnet theorem makes inseparable) is inherently present and, thus, its effect on the LDOS of the graphene sublattices can be neither avoided nor disentangled. In particular notice that the contrast while being off in magnitude is qualitatively the same.

In summary, the Beltrami's pseudosphere tiled by carbon atoms arranged in a defected graphene net may represent a viable analogue model of a quantum field theory in curved space-time in general, and a black-hole horizon in particular. The success of our numerical effort in verifying the analytical predictions obtained within a continuum representation, suggests that this analogue system, if experimentally realized (for example through direct optical forging[24]), can allow measuring a Hawking temperature of the order of tens of K by measuring the surface LDOS through either low temperature Scanning Tunnlling Microscope or optical near-field spectroscopy.

ACKNOWLEDGMENTS

N.M.P. is supported by the European Commission under the Graphene Flagship Core 2 grant No. 785219 (WP14, "Composites") and FET Proactive ("Neurofibres") grant No. 732344 as well as by the Italian Ministry of Education, University and Research (MIUR) under the "Departments of Excellence" grant L.232/2016. The authors acknowledge Bruno Kessler Foundation (FBK) for providing unlimited access to the KORE computing facility.

[1] S. W. Hawking, Black hole explosions, *Nature* **248**, 30 (1974).
[2] W. G. Unruh, Experimental black hole evaporation, *Phys. Rev. Lett.* **46**, 1351 (1981).
[3] T. A. Jacobson, G. E. Volovik, Event horizons and ergoregions in He-3, *Phys. Rev.* **D58**, 064021 (1998).
[4] L. J. Garay, J. R. Anglin, J. I. Cirac, P. Zoller, Black holes in Bose-Einstein condensates, *Phys. Rev. Lett.* **85**, 4643 (2000).
[5] C. Barcelo, S. Liberati, M. Visser, Towards the observation of Hawking radiation in Bose-Einstein condensates, *Int. J. Mod. Phys.* **A18**, 3735 (2003).
[6] S. Giovanazzi, Experimental black hole evaporation, *Phys. Rev. Lett.* **94**, 061302 (2005).
[7] R. Balbinot, A. Fabbri, S. Fagnocchi, A. Recati, I. Carusotto, Non-local density correlations as signal of Hawking radiation in BEC acoustic black holes, *Phys. Rev.* **A78**, 021603 (2008).
[8] I. Carusotto, S. Fagnocchi, A. Recati, R. Balbinot, A. Fabbri, Numerical observation of Hawking radiation from acoustic black holes in atomic BECs, *New J. Phys.* **10**, 103001 (2008).
[9] J. Macher, R. Parentani, Black hole radiation in Bose-Einstein condensates, *Phys. Rev.* **A80**, 043601 (2009).
[10] P. N. Recati, A., I. Carusotto, Bogoliubov Theory of acoustic Hawking radiation in Bose-Einstein Condensates, *Phys. Rev.* **A80**, 043603 (2009).
[11] P. E. Larre, A. Recati, I. Carusotto, N. Pavloff, Quantum fluctuations around black hole horizons in Bose-Einstein condensates, *Phys. Rev.* **A85**, 013621 (2012).
[12] J. Steinhauer, Measuring the entanglement of analogue Hawking radiation by the density-density correlation function, *Phys. Rev.* **D92**, 024043 (2015).
[13] J. Steinhauer, Observation of quantum Hawking radiation and its entanglement in an analogue black hole, *Nature Phys.* **12**, 959 (2016).
[14] J. R. M. de Nova, K. Golubkov, V. I. Kolobov, J. Steinhauer, Observation of thermal Hawking radiation and its temperature in an analogue black hole, *Nature* **569**, 688 (2019).
[15] M. Franz, M. Rozali, Mimicking black hole event horizons in atomic and solid-state systems, *Nature Rev. Mater.* **3**, 491 (2018).
[16] S. Sachdev, J. Ye, Gapless spin fluid ground state in a random, quantum Heisenberg magnet, *Phys. Rev. Lett.* **70**, 3339 (1993).
[17] A. Kitaev, A simple model of quantum holography, *KITP Strings Seminar and Entanglement Program* .
[18] A. Iorio, G. Lambiase, The Hawking-Unruh phenomenon on graphene, *Phys. Lett.* **B716**, 334 (2012).
[19] A. Iorio, G. Lambiase, Quantum field theory in curved graphene spacetimes, Lobachevsky geometry, Weyl symmetry, Hawking effect, and all that, *Phys. Rev.* **D90**, 025006 (2014).

[20] S. Taioli, R. Gabbrielli, S. Simonucci, N. M. Pugno, A. Iorio, Lobachevsky crystallography made real through carbon pseudospheres, *Journal of Physics: Condensed Matter* **28**, 13LT01 (2016).
[21] A. H. Castro Neto, F. Guinea, N. M. R. Peres, K. S. Novoselov, A. K. Geim, The electronic properties of graphene, *Rev. Mod. Phys.* **81**, 109 (2009).
[22] A. Iorio, G. Lambiase, The hawking-unruh phenomenon on graphene, *Physics Letters B* **716**, 334 (2012).
[23] A. Iorio, G. Lambiase, Quantum field theory in curved graphene spacetimes, lobachevsky geometry, weyl symmetry, hawking effect, and all that, *Phys. Rev. D* **90**, 025006 (2014).
[24] A. Johansson, *et al.*, Optical Forging of Graphene into Three-Dimensional Shapes, *Nano Lett.* **17**, 6469 (2017).
[25] A. Kumar, M. Wilson, M. F. Thorpe, Amorphous graphene: a realization of zachariasen's glass, *Journal of Physics: Condensed Matter* **24**, 485003 (2012).
[26] F. Wooten, K. Winer, D. Weaire, Computer generation of structural models of amorphous si and ge, *Phys. Rev. Lett.* **54**, 1392 (1985).
[27] E. Bitzek, P. Koskinen, F. Gähler, M. Moseler, P. Gumbsch, Structural relaxation made simple, *Phys. Rev. Lett.* **97**, 170201 (2006).
[28] H. Gould, J. Tobochnik, W. Christian, An introduction to computer simulation methods (1988).
[29] S. Alfthan, Computational studies of silicon interfaces and amorphous silica, G5 artikkeliväitöskirja (2006).
[30] J. C. Slater, G. F. Koster, Simplified lcao method for the periodic potential problem, *Phys. Rev.* **94**, 1498 (1954).
[31] S. Yuan, M. Rösner, A. Schulz, T. O. Wehling, M. I. Katsnelson, Electronic structures and optical properties of partially and fully fluorinated graphene, *Phys. Rev. Lett.* **114**, 047403 (2015).
[32] T. Stauber, J. I. Beltran, J. Schliemann, Tight-binding approach to penta-graphene, *Scientific Reports* **6**, 22672 (2016).
[33] P. Giannozzi, *et al.*, Quantum espresso: a modular and open-source software project for quantum simulations of materials, *Journal of Physics: Condensed Matter* **21**, 395502 (2009).
[34] A. Weiße, G. Wellein, A. Alvermann, H. Fehske, The kernel polynomial method, *Rev. Mod. Phys.* **78**, 275 (2006).
[35] J. Garcia, The kernel polynomial method for quantum transport in disordered systems, Ph.D. thesis (2015).

METHODS

Tiling the pseudosphere

The tiling of the Beltrami's pseudosphere by carbon atoms, which represents an interesting geometrical problem on its own right, has been achieved through the following steps:

1. Set the length of the pseudosphere by fixing the maximum value of the coordinate along the axis of revolution (z).

2. Determine the number of carbon atoms N that are needed if one were to tile the surface of the Beltrami's pseudosphere with the same density of planar graphene (0.379 atoms/Å^2). Periodic boundary conditions are also introduced to saturate the outer carbon atom bonds belonging to $r = R_{\rm p}$ and $z = 0$ (the Hilbert horizon); finally, a rectangular supercell periodically repeated along the x and y directions, respectively.

3. Construct a planar graph (N, F, E) consisting of N vertices, F faces and E edges. The N vertices represent compressed carbon atoms with shortened carbon-to-carbon bond lengths, $a_{\rm CC}$ <1.42 Å; each vertex is linked to three nearest neighbours by edges (representing bonds) and is shared by three faces.

4. Map the initial graph onto the Beltrami's pseudosphere surface via a one-to-one transformation, by which the revolution axis coordinate z of the vertices is unambiguously determined $\forall\sqrt{x^2+y^2} < R_p$ by fixing

$$z = z(x,y) = R\left[\sqrt{1-\frac{x^2+y^2}{R_{\rm p}^2}} - \operatorname{atanh}\sqrt{1-\frac{x^2+y^2}{R_{\rm p}^2}}\,\right];$$

5. Find the atomic arrangements with $N \sim$ 1000-2000 that minimize a surface potential energy of the Keating type[25]:

$$E = \frac{3}{16}\frac{\alpha}{a_{\rm CC}^2}\sum_{i,j}\left(r_{ij}^2 - a_{\rm CC}^2\right)^2 + \frac{3}{8}\frac{\beta}{a_{\rm CC}^2}\sum_{i,j,k}\left(\mathbf{r}_{ij}\cdot\mathbf{r}_{ik} + \frac{a_{\rm CC}^2}{2}\right)^2 + c_h\sum_{F_i}(|F_i|-6)^2 \qquad (4)$$

where $\alpha = 25.88$ eV Å $^{-2}$ is the bond stretching force constant, $a_{\rm CC} = 1.42$ Å is the carbon-to-carbon bond length in planar graphene, r_{ij} is the distance between atoms i and j, and $\beta \sim \frac{\alpha}{5}$ is the bond–bending force

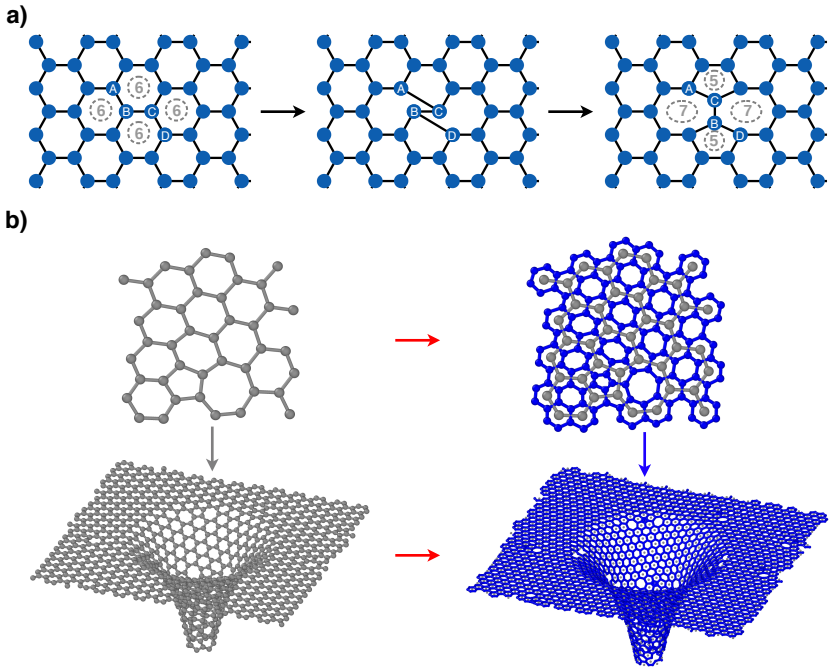

FIG. 5. a) An example of a bond-switch trial move in a graphene lattice. Starting from an initial configuration showing 6-fold rings (dashed circles), the bonds between the carbon atoms A–B, and C–D are cut, and new bonds A–C and B–D are formed. Twisting then transforms the four 6-fold rings into two 5-fold rings and two 7-fold rings (adapted from Ref.[29]). b) Dualization sequence based on the three-connectivity of the graph. The parent parent geometry is shown on the left, while the resulting (daughter) geometry is on the right.

constant. The last term favours the formation of hexagonal faces; as F_i labels the polygons of the net $|F_i|$ is the number of vertices of the polygons ($c_h = 0.35$ empirically). To reach the energy minimum repeat the following steps, typically $\mathcal{O}(10^4)$ times:

- perform random switchings/twists of atomic bonds, based on the Wooten, Winer and Weaire (WWW) method[26] (Fig. 5 a);
- let the geometry relax through molecular dynamics simulations based on the Fast Inertial Relaxation Engine (FIRE) approach[27];
- accept the move only if it lowers the total energy of the system according to a Metropolis algorithm[28].

6. Execute on the minimized surfaces a dualization sequence, to increase the number N of atoms and correspondingly the radius of the pseudosphere ((Fig. 5 b). By using the three-connectivity of the graph one creates a hexagon around each vertex of the initial optimized structure; rescale the bond lengths with a $\sqrt{3}$ factor and repeat from 5.

Tight Binding parameter estimate

Low energy electronic properties of geometries containing millions of atoms, have been evaluated using a TB approach, which is well known to describe correctly the dispersion of graphene around the six Dirac K-points in the first Brillouin zone (IBZ)[21]. Due to the pseudosphere curvature, a multi-orbital TB approach has been developed, in which all four valence orbitals $(2s, 2p_x, 2p_y, 2p_z)$ are included in the simulation through the Hamiltonian:

$$H = \sum_{\xi i} \epsilon^i_\xi a^\dagger_{i,\xi} a_{i,\xi} + \sum_{\xi,\gamma\langle ij\rangle} t^{ij}_{\xi,\gamma} a^\dagger_{i,\xi} a_{j,\gamma}, \tag{5}$$

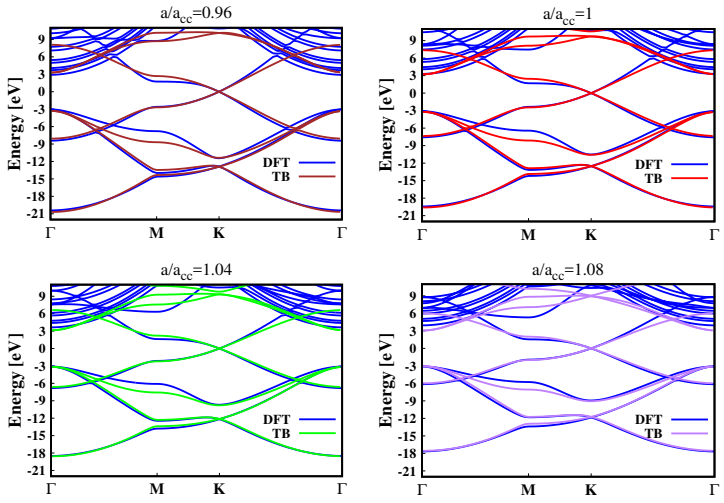

FIG. 6. TB fit of graphene bands obtained from DFT electronic structure calculations. From left to right and from top to bottom we report the bands for a biaxial compression of the graphene cell equal to 4 %, unstrained graphene, and a biaxial tensile strain of the cell equal to 4 %and 8%.

where ξ, γ are orbital label indices while i, j are site indices; $t^{ij}_{\xi,\gamma}$ indicates the hopping parameters; and the symbol $\langle ij \rangle$ means that the nearest neighbours approximation is adopted. The parameters $t^{ij}_{\xi,\gamma}$ describing the hopping between orbitals in different sites were computed within the Slater-Koster formulation[30], which provides a scheme to relate the orbital symmetry, distances and directions of neighbour atoms. Owing to the non-planarity of our geometry we cannot make use of the multi-orbital parametrization typically used for graphene[31,32] where the onsite energy of the p_z-symmetry orbitals are treated differently from the x, y orbital cartesian components along the in-plane directions (that is $\epsilon_{p_x} = \epsilon_{p_y} \neq \epsilon_{p_z}$). Therefore, we derive the TB parameters by fitting ab-initio Density Functional Theory (DFT) simulations of the graphene bands by further imposing that the onsite energies for the p orbitals are the same ($\epsilon_{p_x} = \epsilon_{p_y} = \epsilon_{p_z}$). DFT simulations of equilibrium and strained configurations of graphene were carried out by using the Quantum Espresso code suite[33]; in particular we use a norm–conserving PBE pseudopotential (C.pbe-mt gipaw.UPF) and an energy cut-off for the wavefuntion expansion on plane-waves set equal to 100 Ry. The k-point mesh is a 40401 grid for the calculation of both the ground state density and the band structures. Convergence of the integrals over the Brillouin zone was improved by smearing the occupancy with a 0.136 eV width Gaussian function. The TB parameters that we obtained using Eq. (5) for unstrained ($a \equiv a_{\rm CC}$) and strained graphene ($a \neq a_{\rm CC}$) are (see Fig. 6): $\epsilon_s = -2.8$ eV and $\epsilon_p = 0$ eV as onsite energies; $V_{ss\sigma}(a) = -5.6 \cdot a \neq a_{\rm CC} \cdot e^{-\frac{a-a_{\rm CC}}{0.55}}$ eV, $V_{sp\sigma}(a) = 5.2 \cdot a/a_{\rm CC} \cdot e^{-\frac{a-a_{\rm CC}}{0.75}}$ eV, $V_{pp\sigma}(a) = 4.6 \cdot a/a_{\rm CC} \cdot e^{-\frac{a-a_{\rm CC}}{0.55}}$ eV and $V_{pp\pi}(a) = -2.44 \cdot a/a_{\rm CC} \cdot e^{-\frac{a-a_{\rm CC}}{0.41}}$ eV as hopping parameters between different orbitals.

Kernel Polynomial Method

For the evaluation of the Local Density of States (LDOS) we resorted to The Kernel Polynomial Method (KPM), which is a numerical approach useful to access spectral quantities of extended systems for which a direct diagonalization of the full Hamiltonian matrix is computationally unfeasible. It consists in the expansion of the sought quantity in terms of a set of orthogonal polynomials, and then in improving the convergence of the expansion with a kernel to avoid spurious Gibbs oscillations[34]. In particular, we used Chebyshev polynomials for the expansion, and Jackson kernel to increase convergence, resolution, and accuracy[34]. Under these conditions a generic function can be expanded according to

$$f(x) = \frac{1}{\pi\sqrt{1-x^2}} \left[\mu_0 g_0 + \sum_{n=1}^{N_c - 1} \mu_n g_n T_n(x) \right], \tag{6}$$

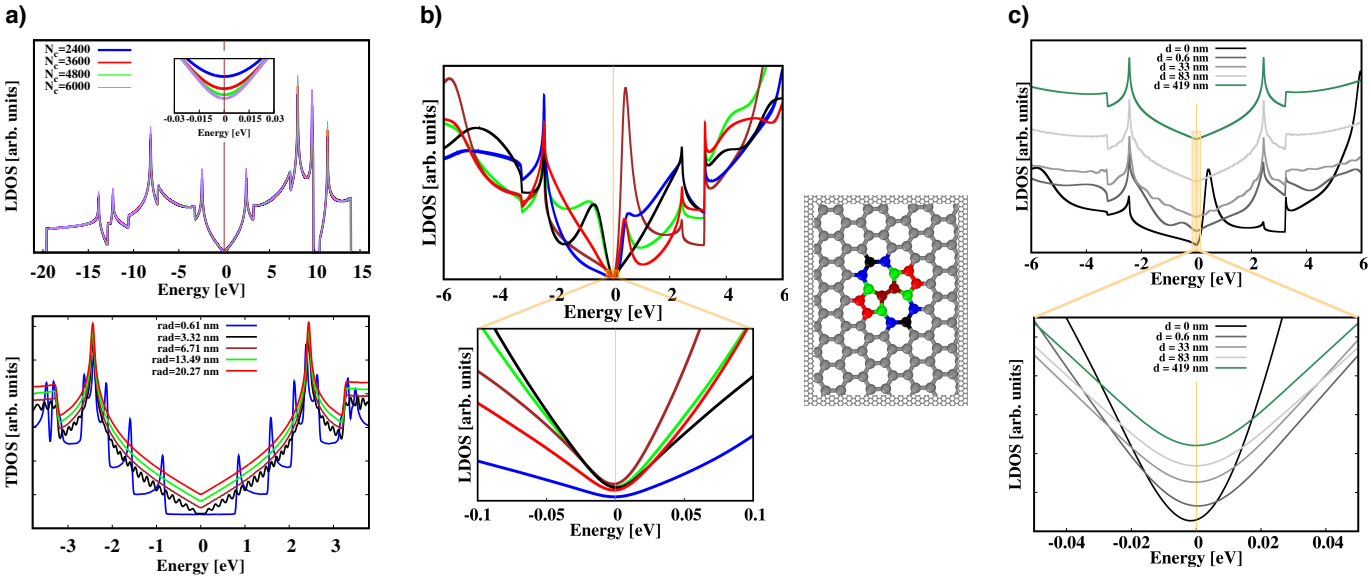

FIG. 7. a) (top) LDOS for different values of the cut-off parameter N_c obtained by projection on a site of a pristine graphene rectangular cell with sides equal to 199.97 nm × 199.81 nm, containing 1,525,188 carbon atoms; The inset represents a zoom near the Fermi energy. (bottom) total DOS of (n,n) nanotubes for n=9 ($r = 0.61$ nm), n=49 ($r = 3.32$ nm), n=99 ($r = 6.71$ nm), n=199 ($r = 13.49$ nm) and n=299 ($r = 20.27$ nm). b) The LDOS angular and radial dependence obtained by projecting over sites belonging to a SW defect (colored atoms in the right panel). c) The LDOS radial dependence.

where $T_n(x)$ are Chebyshev polynomials of the first kind, $\mu_n = \int_{-1}^{1} \mathrm{d}x\, f(x) T_n(x)$ are the coefficients of the expansion and the g_n are the Jackson kernel coefficients defined as

$$g_n = \frac{1}{N_c+1}\left[(N_c - n + 1)\cos\frac{\pi n}{N_c+1} + \sin\frac{\pi n}{N_c+1}\cot\frac{\pi}{N_c+1}\right], \tag{7}$$

with N_c the truncation number related to the maximum momentum. The best achievable resolution through this kernel is

$$\Delta^J = \sqrt{1 - \cos\frac{\pi}{N_c+1}}. \tag{8}$$

We refer to[34] for the details about the calculation of μ_n; here it suffices to emphasize that it is based on the Stochastic Evaluation of Traces, which requires a certain number R of random initial states. As expected, the bigger is R, the more accurate becomes the evaluation of the coefficients; we found that $R = 100$ was enough for all calculations carried out.

Tests of the LDOS calculation

The convergence with respect to the N_c parameter can be tested in the calculation of the LDOS for the benchmarks cases of planar graphene and armchair carbon nanotubes. The LDOS for four different values of N_c ranging from 2400 to 6000, is shown in Fig. 7 a) top. While at a wide energy scale the curves are indistinguishable, zooming near the Fermi energy (set to zero as usual), shows higher truncation values for N_c captures more faithfully the expected linear dispersion relation; on the other hand, there is a threshold to the number of terms in the summation after which spurious oscillations sets is, spoiling convergence. This can be understood by noticing that the energy separation between levels in periodic graphene is infinitesimal and the DOS is a continuous function. Then, since the pseudosphere in our simulations is a large but finite system and the energy separation of the levels increases with respect to infinite periodic structures, a too big value of N_c may result in a KPM energy resolution marginally above the finite energy separation between levels of our finite system, thus leading to poor convergence[35]. For non-planar systems, we have computed the total DOS of (n,n) nanotubes for $n = 9,\ 99,\ 199$ and 299 (radius $r = 0.61,\ 3.32,\ 6.71$

and 13.49 nm). The total DOS is reported in the bottom panel of Fig. 7 a), where we observe that the DOS lineshape of these armchair nanotubes is reproduced surprisingly well already for the moderate value of $N_c = 2000$ and that, as expected, the confinement effects become less important upon increasing the radius size.

Since a method for estimating the value of N_c that trades-off between accuracy and computational efficiency exists only for pristine structures that do not have any defect[35], selecting the best N_c is a trial and error process. For the pseudosphere case we found $N_c = 8000$ to be the optimal value (with $N_c = 16000$ used when resolving the Fermi energy region in Fig. 4).

LDOS of a single SW defect in planar graphene

Let us finally investigate the effect of the presence of a single Stone-Wales (SW) defect, like the ones present in the pseudosphere, on the LDOS of a graphene net ($N = 823,860$). In particular, we study both the LDOS projected over different symmetry sites of the SW defect (with $N_c = 5000$), thus obtaining information on the angular dependence (Fig. 7 b), as well as the LDOS projected over sites increasingly far from the SW defect, thus obtaining insights on the radial dependence (Fig. 7 c). On top of a marked angular dependence, we see that the shape of the LDOS is dramatically modified near the defect site, while far from it the planar graphene shape is recovered; the presence of the SW defect still affects the LDOS projected at distances of ≈ 80 Å with small oscillations in the spectrum. Near the Fermi energy one observes in addition a marked asymmetry persisting again up to a distance of ≈ 80 Å .